ADVANCED MATERIALS
www.advmat.de

Slip-Line-Guided Growth of Graphene

Yanglizhi Li, Haiyang Liu, Zhenghua Chang, Haoxiang Li, Shenxing Wang, Li Lin, Hailin Peng, Yujie Wei, Luzhao Sun,* and Zhongfan Liu**

Manipulating the crystal orientation of emerging 2D materials via chemical vapor deposition (CVD) is a key premise for obtaining single-crystalline films and designing specific grain-boundary (GB) structures. Herein, the controllable crystal orientation of graphene during the CVD process is demonstrated on a single-crystal metal surface with preexisting atomic-scale stair steps resulting from dislocation slip lines. The slip-line-guided growth principle is established to explain and predict the crystal orientation distribution of graphene on a variety of metal facets, especially for the multidirectional growth cases on Cu(*hk*0) and Cu(*hkl*) substrates. Not only large-area single-crystal graphene, but also bicrystal graphene with controllable GB misorientations, are successfully synthesized by rationally employing tailored metal substrate facets. As a demonstration, bicrystal graphenes with misorientations of ≈21° and ≈11° are constructed on Cu(410) and Cu(430) foils, respectively. This guideline builds a bridge linking the crystal orientation of graphene and the substrate facet, thereby opening a new avenue for constructing bicrystals with the desired GB structures or manipulating 2D superlattice twist angles in a bottom-up manner.

1. Introduction

The main principle of epitaxy, which emphasizes the lattice match between the epilayer and underlying crystalline substrates, has successfully guided the synthesis of single-crystal metals, semiconductors, and dielectric thin films in modern industry.[1] Current research on the controllable epitaxy of emerging 2D materials provides new opportunities for enriching the conventional epitaxy principle. Compared with that of bulk materials, the epitaxial behavior of 2D materials is quite different owing to their unique interfacial structures. For instance, during the growth of graphene on metal substrates, the intralayer covalent bonds together with no surface dangling bonds give rise to weak graphene surface–metal substrate interaction. The graphene edge-metal step interaction is regarded as a key factor for determining the alignments of graphene on a metal surface.[2–4] A pioneering study also revealed that step-edge complementarity enables the growth of 2D single crystals.[5] Furthermore, the close-packed <110> or <211> steps on face-centered cubic (FCC) metal surfaces were proven to have a strong binding with the edges of 2D materials, thereby enabling the unidirectional growth of hexagonal boron nitride[6,7] and MoS_2[8] on vicinal Cu(110)/Cu(111) and Au(111) facets, respectively. The step-edge epitaxy is also applicable to the growth of borophene.[9] Recently, based on the systematic analysis of interactions between 2D materials and ideal metal surface structure, a symmetry rule was put forward, revealing that the unidirectional growth occurs when the symmetric group of the metal surface belongs to a subgroup of that of the 2D materials.[10] Specifically, the substrate should have C_{6V}, C_{3V}, C_{2V}, or C_1 symmetry to enable the unidirectional growth of graphene with C_{6V} symmetry.

Y. Li, H. Liu, S. Wang, H. Peng, Z. Liu
Center for Nanochemistry
Beijing Science and Engineering Center for Nanocarbons
Beijing National Laboratory for Molecular Sciences
College of Chemistry and Molecular Engineering
Peking University
Beijing 100871, P. R. China
E-mail: zfliu@pku.edu.cn

Y. Li
Academy for Advanced Interdisciplinary Studies
Peking University
Beijing 100871, P. R. China

Y. Li, H. Liu, H. Li, S. Wang, L. Lin, H. Peng, L. Sun, Z. Liu
Beijing Graphene Institute
Beijing 100095, P. R. China
E-mail: sunlz-cnc@pku.edu.cn

Z. Chang, Y. Wei
LNM
Institute of Mechanics
Chinese Academy of Sciences
Beijing 100190, P. R. China
E-mail: yujie_wei@lnm.imech.ac.cn

Z. Chang, Y. Wei
School of Engineering Sciences
University of Chinese Academy of Sciences
Beijing 100049, P. R. China

L. Lin
School of Materials Science and Engineering
Peking University
Beijing 100871, P. R. China

The ORCID identification number(s) for the author(s) of this article can be found under https://doi.org/10.1002/adma.202201188.

DOI: 10.1002/adma.202201188

While scientists have long sought to understand and control the epitaxy of 2D materials, several bottlenecks/contradictions remain owing to the far more complex experimental reality of metal surface compared with that considered in previous studies: I) Explaining and predicting the dominant orientations of graphene grown on arbitrary metal facets is extremely challenging. Graphene domains do not grow unidirectionally on the Cu(110) facet[11] (C_{2V} symmetry) and many high-index facets of low rotational symmetry, but exhibit two or more preferential orientations. This fact does not support simple symmetry rules.[10] Such phenomena cannot be explained by current growth theory, indicating that some key factors beyond symmetry must be clarified. II) The arbitrary control of the crystal orientation of graphene domains for maneuvering 2D grain-boundaries (GBs) structures[12] is hardly possible due to the lack of a comprehensive understanding of 2D materials growth and the key determining factors of graphene orientation. Because the previous studies mainly focus on ideal metal surfaces, deeper insights into the real surface structure of metals, especially surface reconstruction at high temperatures, are essential to understand the epitaxy of 2D materials.

Herein, we consider the slip phenomenon, a type of imprint left by dislocation annihilation during high-temperature annealing, of metal substrates to clarify the epitaxial growth behavior of graphene. It was found that the slip lines on metal surfaces are crucial for guiding the growth of graphene, determining its crystal orientation, and explaining the orientation distributions of graphene grown on a variety of Cu facets. Density functional theory (DFT) calculations confirmed that the graphene domains are prone to aligning with slip lines or intrinsic steps which have high binding energy in graphene edge–metal step configurations. The slip-line-guided growth principle was established for predicting the possible epitaxial orientations of graphene domains on arbitrary Cu(*hkl*) facets. As a demonstration, bicrystal graphene domains with designed GB structures were successfully prepared by the rational design of metal substrates with specific crystal facets.

2. Results and Discussion

Slip lines caused by dislocation annihilation during high-temperature annealing are commonly observed in Cu foils/films produced by cold rolling or sputtering process, leading to the deviation of surface structures from the ideal models with intrinsic metal steps.[13] During the subsequent chemical vapor deposition (CVD) process, these lines play an essential role in determining the crystal orientation of the graphene domains. Uni- or multidirectional growth occurs depending on the number of active slip lines on the metal surface (**Figure 1**a). In detail, we systematically examined the crystal orientations of graphene domains grown on single-crystal Cu foils with various facets, based on our previously established strain-engineered anomalous grain growth method.[14,15] Typically, the Cu(211) facet was determined by electron backscattering diffraction (EBSD) measurements, and three sets of slip lines were detected on this facet by atomic force microscopy (AFM). The measured internal angles of the triangle formed by the slip lines are 44°, 68°, and 68° (Figure 1b). The graphene domains on Cu(211) grow unidirectionally with one edge aligned along the $[0\bar{1}1]$ direction (Figure 1c). Statistically, these graphene domains exhibit one prominent orientation with very few cases of ≈30° misorientated domains (0.6%), which is consistent with previous reports on aligned graphene growth (Figure 1d).[16,17] Subsequently, the graphene domains were transferred onto a transmission electron microscopy (TEM) grid for further accurate orientation determination via selected area electron diffraction (SAED). Only one set of SAED patterns was obtained from different graphene domains, thus confirming the high orientation consistency of graphene (Figure S1a–d, Supporting Information). However, the multidirectional growth of graphene occurs on certain high-index facets despite the low symmetry of these substrates. For instance, on the Cu(410) facet with four sets of slip lines (Figure 1e), the graphene domains show three dominant orientations as indicated by the red, blue, and yellow dashed lines in Figure 1f. In the corresponding statistical results of the edge orientations, three prominent peaks with an interval of ≈40° could clearly be observed (lattice orientation difference, ≈20°), along with some misoriented domains (Figure 1g). The SAED results display three sets of diffraction patterns with ≈20° mutual lattice orientation differences among different graphene domains (Figure S1e–h, Supporting Information), being in good agreement with the statistical results.

The unique orientation distributions of graphene domains on distinct high-index facets cannot be explained by considering only the symmetry or ideal structures of metal surfaces. An in-depth exploration of the slip-induced surface reconstruction is crucial for solving the puzzles. For the FCC metal Cu, dislocations reside on the {111} close-packed crystallographic planes and glide in the <110> directions, that is, the twelve slip systems {111}<110> (Figure S2, Supporting Information). As a consequence, slip-induced steps form on the crystal surface after atomic rearrangements (**Figure 2**a). The detailed orientations of the slip lines on arbitrary metal facets can be calculated, and their distribution rules are summarized in Note S1, Supporting Information. To describe the orientation distribution of slip lines on the crystal surface (*hkl*) in greater detail, we used a specific surface (herein (410) facet is selected for illustration) to slice the octahedron composed of {111} slip planes and obtained its cross-sectional profile. Each boundary of the quadrilateral section represents a set of slip lines (Figure 2b). An atomic model of the Cu(410) surface is then constructed with four sets of slip-induced steps along the $[1\bar{4}3]$, $[1\bar{4}\bar{3}]$, $[1\bar{4}\bar{5}]$, and $[1\bar{4}5]$ directions and one set of intrinsic steps along the [001] direction. The theoretical internal angles of the quadrilateral formed by the slip lines on Cu(410) are 72°, 93.5°, 101°, and 93.5°, which are consistent with the experimental values shown in Figure 1e. **Table 1** shows the theoretical crystal orientation of the slip lines on typical metal facets, as confirmed by EBSD and AFM measurements (Figure S3, Supporting Information).

With the detailed distribution rules of slip lines in hand, we explored the relationship between the graphene orientation and slip lines. In the case of unidirectional growth represented by graphene on the Cu(211) surface, one set of graphene edges was found to keep parallel with $[0\bar{1}1]$ slip line (referred to as active slip line in this work). By contrast, the $[2\bar{1}\bar{3}]$ and $[2\bar{3}\bar{1}]$ slip lines show no activity toward guiding the growth of graphene (referred to as inactive slip lines in this work). Consequently,

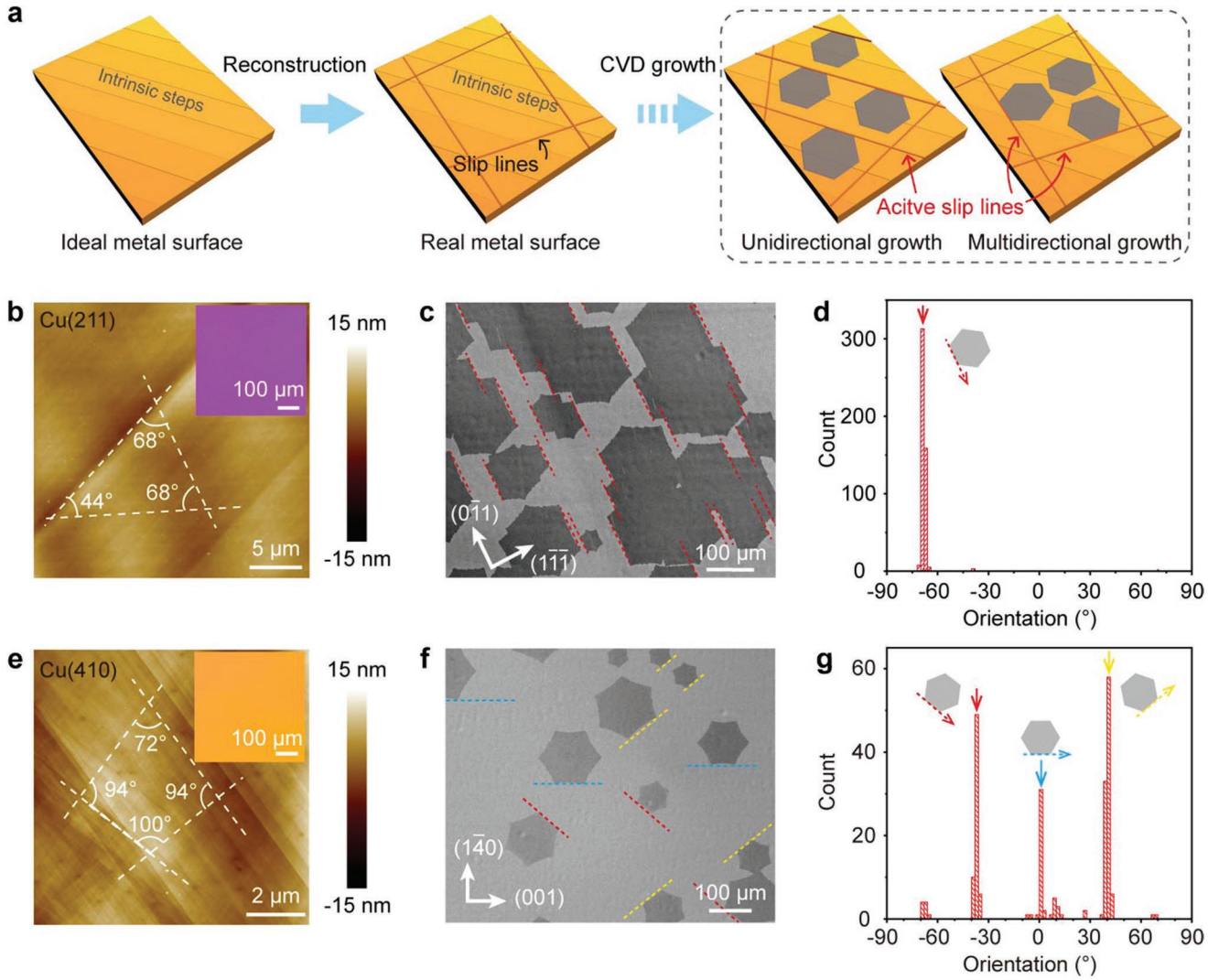

Figure 1. The slip-line-guided growth of graphene. a) Schematic illustration of the slip-line-guided growth principle. The crystal orientations of graphene are mainly determined by those of the active slip lines. b) AFM image of the Cu(211) foil. The slip lines are highlighted by white dotted lines. Inset: the corresponding EBSD IPF map. c) SEM image of graphene domains on the Cu(211) foil. d) Statistics of the crystal orientation of graphene on the Cu(211) foil. e) AFM image of the Cu(410) foil. The slip lines are highlighted by white dotted lines. Inset: the corresponding EBSD IPF map. f) SEM image of graphene domains on the Cu(410) foil. g) Statistics of the crystal orientation of graphene on the Cu(410) foil.

unidirectional growth could be attributed to the existence of a single set of active slip lines (Figure S4a,b, Supporting Information). A similar result was also observed on the Cu(221) surface, where the [1$\bar{1}$0] slip line guides the growth of the aligned graphene domains (Figure S4c,d, Supporting Information).

Interestingly, slip lines also account for the multidirectional growth of graphene domains. For instance, the close-packed <110> and <211> directions do not exist on the Cu(410) surface. Instead, the graphene domains prefer to be aligned with the [1$\bar{4}$5] and [14$\bar{5}$] slip lines together with [001] intrinsic steps, resulting in three dominant orientations. Meanwhile, the [1$\bar{4}\bar{3}$] and [14$\bar{3}$] slip lines on Cu(410) were found to be inactive ones (Figure 2c–f). Since the theoretical values of $\theta_{[001]-[1\bar{4}5]}$ (i.e., the included angle between the [001] and [1$\bar{4}$5] directions, similarly hereinafter) and $\theta_{[001]-[14\bar{5}]}$ are 39.5° and 39.5°, the orientation difference between corresponding graphene domains should be 20.5° and 20.5° (60–39.5°), respectively, which agrees well with the statistical results shown in Figure 1g.

Analogously, the majority of graphene domains on the Cu(430) surface are aligned with the [3$\bar{4}$7] and [3$\bar{4}\bar{7}$] slip lines together with a minor part aligned with the [001] intrinsic step, while the [3$\bar{4}$1] and [3$\bar{4}\bar{1}$] slip lines keep inactive. On the Cu(431) facet, the graphene domains are mainly guided by the [4$\bar{5}\bar{1}$] and [4$\bar{3}\bar{7}$] slip lines rather than the [2$\bar{3}$1] and [2$\bar{5}$7] slip lines. On the Cu(621) facet, the active slip lines are along the [1$\bar{7}$8], [3$\bar{5}\bar{8}$] and [3$\bar{7}\bar{4}$] directions, among which the [1$\bar{7}$8] slip line is the most active. For the Cu(821) facet, all four sets of slip lines guide the growth of graphene, and the majority of graphene domains are dominated by the [1$\bar{9}$10] slip line (Figure S5, Table S1, Supporting Information).

DFT calculations were employed to understand the alignment of the graphene edges with the slip lines. Herein, a

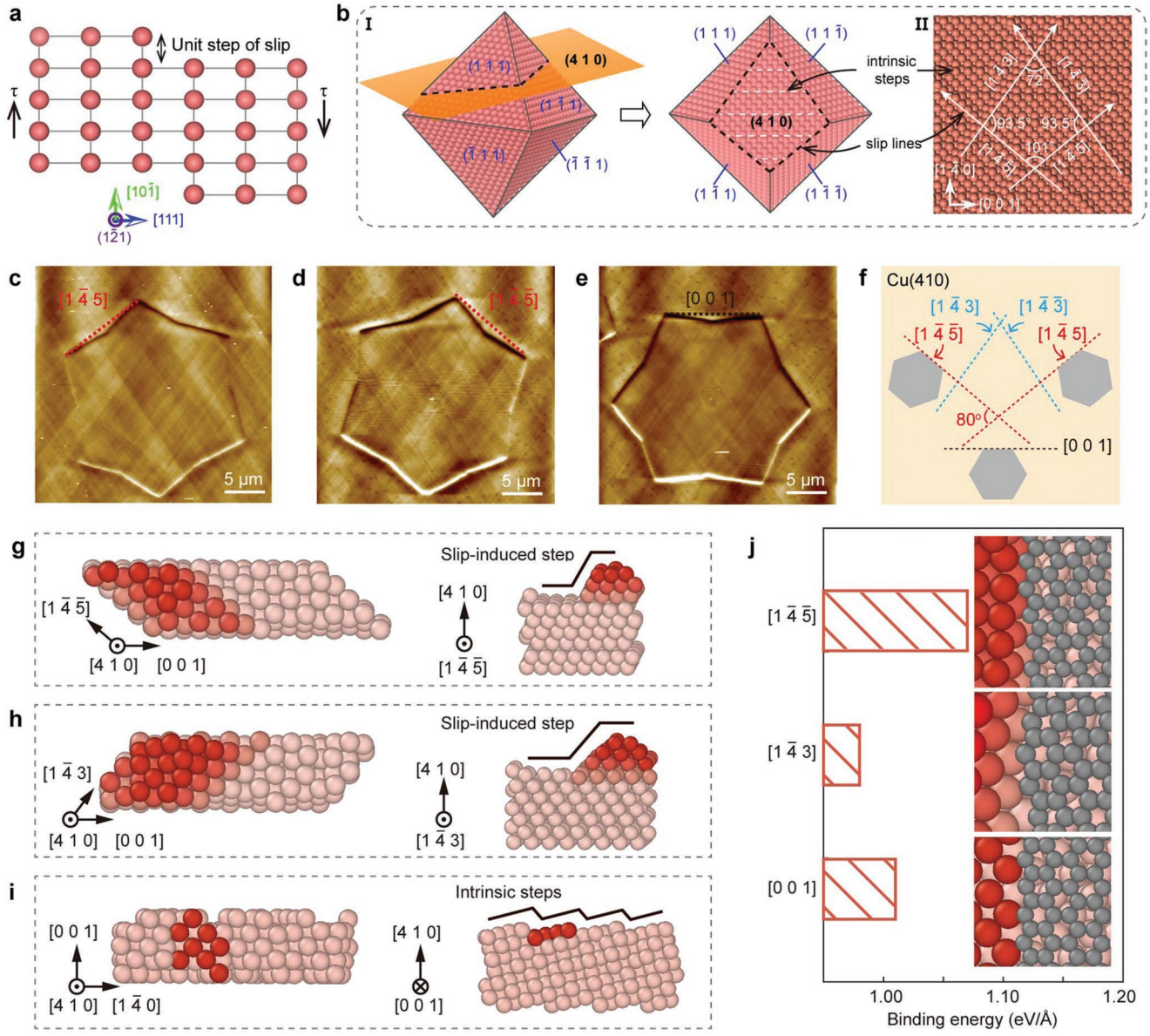

Figure 2. The determining role of slip lines in guiding the graphene growth. a) The formation of the slip-induced steps after the atomic rearrangements along the (111)[10$\bar{1}$] direction. b) Schematic illustration of determination of the orientation of slip lines on FCC metal surface (I) and the corresponding atomic model of the Cu(410) surface with the slip-induced steps and the intrinsic steps (II). c–e) AFM images of graphene domains aligned with the [1$\bar{4}$5] (c), [1$\bar{4}\bar{5}$] (d), and [001] (e) steps on the Cu(410) facet. f) Schematic illustration of the graphene domains aligned with the [1$\bar{4}\bar{5}$], [1$\bar{4}$5], and [001] steps rather than the [1$\bar{4}\bar{3}$], [1$\bar{4}$3] steps on the Cu(410) facet. g,h) Top (on the left) and lateral (on the right) views of Cu(410) substrates with the slip-induced steps along the [1$\bar{4}$5] (g) and [1$\bar{4}$3] (h) directions and i) of a pristine Cu(410) substrate with the intrinsic step along the [001] direction. j) Binding energies between graphene edges and Cu(410) substrates with different types of steps from DFT calculations.

typical Cu(410) substrate was chosen for general demonstration. The top and lateral views of Cu(410) substrates with slip-induced steps along the [1$\bar{4}$5] and [1$\bar{4}$3] directions are shown in Figure 2g,h, respectively. The pristine Cu (410) substrate with [001] steps is shown in Figure 2i. The binding energies between the graphene edge and the Cu[1$\bar{4}\bar{5}$], Cu[1$\bar{4}$3], and Cu[001] steps are calculated to be 1.07, 0.98, and 1.01 eV Å^{-1}, respectively (Figure 2j). For a nanoscale graphene island, the binding energy differences among different steps will reach the scale of several eV, which are sufficient to influence the alignment of graphene.[10] The strongest interaction between the graphene edges and the Cu[1$\bar{4}$5] steps (active slip line) accounts for their leading role in guiding the crystal orientation of graphene. Apart from the contribution of moderate binding energy, the intrinsic Cu[001] steps are capable of guiding the graphene growth owing to their large density. The Cu[1$\bar{4}$3] steps are the least favorable ones in terms of low binding energy and low density compared with intrinsic Cu[001] steps. Therefore we rarely see graphene islands along the Cu[1$\bar{4}$3] steps in experiments. On the Cu(211) facet, the Cu[01$\bar{1}$] steps have stronger

Table 1. The crystal orientation of slip lines on typical crystal facets with different Miller indexes.

Category	Typical crystal facet	Slip line 1[a)]	Slip line 2[a)]	Slip line 3[a)]	Slip line 4[a)]
Basal facet	(100)	$[0\bar{1}1]$	$[0\bar{1}1]$	$[\ 0\bar{1}\bar{1}\ ]$	$[0\bar{1}\bar{1}]$
Basal facet	(111)	-	$[0\bar{1}1]$	$[10\bar{1}]$	$[1\bar{1}0]$
Basal facet	(110)	$[1\bar{1}0]$	$[1\bar{1}2]$	$[1\bar{1}2]$	$[1\bar{1}0]$
(*hkk*)	(211)	$[0\bar{1}1]$	$[0\bar{1}1]$	$[2\bar{1}\bar{3}]$	$[2\bar{3}\bar{1}]$
(*hhk*)	(221)	$[1\bar{1}0]$	$[1\bar{3}4]$	$[3\bar{1}\bar{4}]$	$[1\bar{1}0]$
(*hk*0)	(410)	$[1\bar{4}3]$	$[1\bar{4}5]$	$[1\bar{4}5]$	$[1\bar{4}3]$
(*hkl*)	(431)	$[2\bar{3}1]$	$[2\bar{5}7]$	$[4\bar{3}7]$	$[4\bar{5}\bar{1}]$

[a)]The slip lines 1, 2, 3, and 4 are formed by (111), $(\bar{1}11)$, $(1\bar{1}1)$, and $(\bar{1}\bar{1}1)$ slip planes, respectively.

binding with graphene edges than that of the Cu[$2\bar{1}\bar{3}$] steps, leading to the unidirectional growth of graphene (Figure S6, Supporting Information).

The introduction of active slip lines well explains the orientation distribution of graphene on various metal facets, as shown in **Figure 3**a and Figure S7, Supporting Information. In brief, the unidirectional growth of graphene occurs on the metal facets with one set of active slip lines, such as vicinal Cu(111) (e.g., Cu(111), Cu(776), Cu(765), Cu(654), etc.), Cu(*hkk*) (e.g., Cu(533), Cu(211), etc.), and Cu(*hhk*) (e.g., Cu(332), Cu(331), etc.) facets, as highlighted by the blue shadow in Figure 3a. On the Cu(*hk*0) (e.g., Cu(410), Cu(430), etc.) or partial Cu(*hkl*) (e.g., Cu(621), Cu(431), Cu(821), etc.) facets, multidirectional growth occurs with two, three, or even more dominant orientations, which is attributed to the existence of multiple sets of active slip lines (red shadow in Figure 3a). In the multidirectional growth cases, the edge orientation differences of the distinct graphene domains also depend on the orientation differences of corresponding active slip lines (Figures S5,S8, Supporting Information).

The slip-line-guided growth principle was established based on the above investigations, as summarized in Figure 3b. The graphene domains tend to align with active slip lines possessing high binding energy with the graphene edges. I) On Cu(*hkk*) or Cu(*hhk*) facets (excluding vicinal Cu(100) or vicinal Cu(110) facets), the graphene domains grow unidirectionally because one set of slip lines coincides with the close-packed <110> directions; II) On Cu(*hk*0) facets, the graphene domains incline to grow multidirectionally with two major orientations aligned along two sets of active slip lines and a small part aligned along the (001) intrinsic steps. III) On Cu(*hkl*) facets, the graphene domains may have one, two, or more dominant orientations, depending on the number of active slip lines. For example, vicinal (111) facets usually have one set of active slip lines, while vicinal (100) and vicinal (110) facets have two or more. Based on the geometric analysis of slip-induced steps, the most probable orientation of graphene domains on arbitrary metal facets can be conveniently identified by selecting the active slip lines with the smallest deviation angle with respect to the close-packed <110> or <211> directions (Figure S9, Notes S1,S2, Supporting Information). Because the binding energy between the graphene edge and metal step is not simply linearly related to the deviation angle, slip lines with relatively larger deviation angles may also guide the growth of a certain proportion of graphene domains. A strict and complete estimation requires a detailed calculation of the binding energies on the given crystal facets.

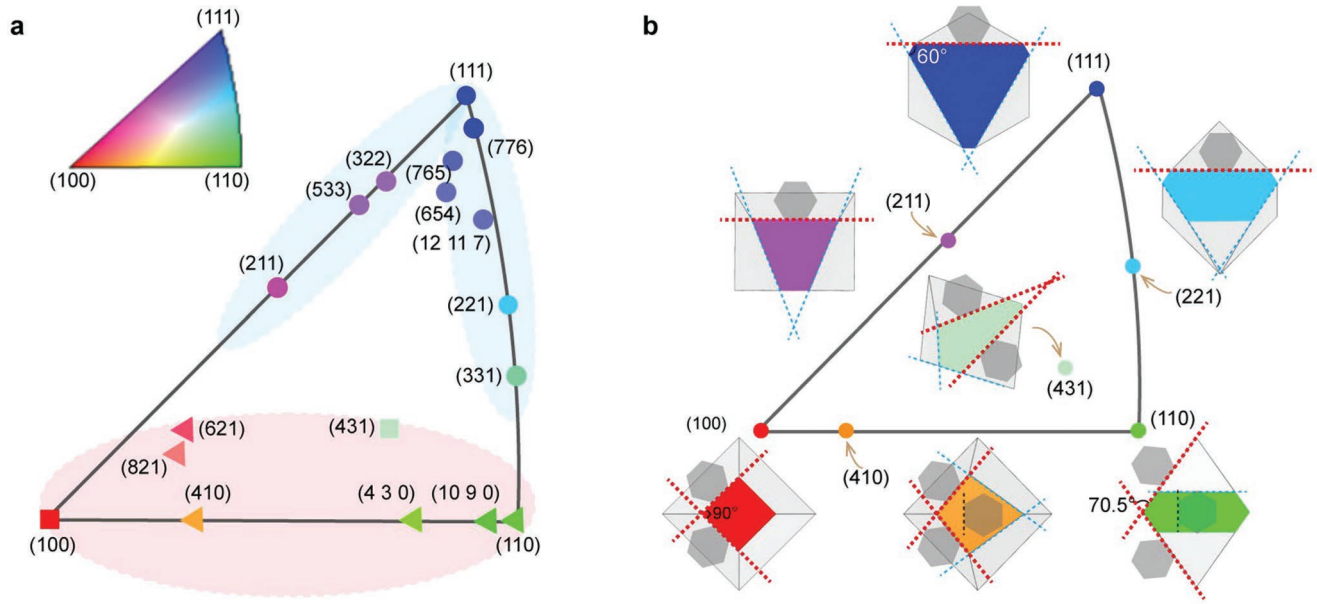

Figure 3. The general orientation distribution rule of graphene grown on a variety of metal facets. a) The experimental orientation distribution rule of the graphene grown on various Cu facets. The circle, square, and triangle represent one, two, and more than or equal to three dominant orientations, respectively. The red and blue shadows denote the case of multi-directional and unidirectional growth, respectively. b) Schematic patterns of active slip lines, inactive slip lines, and intrinsic <100> steps (highlighted by red, blue, and black dotted lines, respectively) on typical metal facets in IPF. The crystal orientations of graphene domains (grey hexagons) are mainly determined by those of active slip lines.

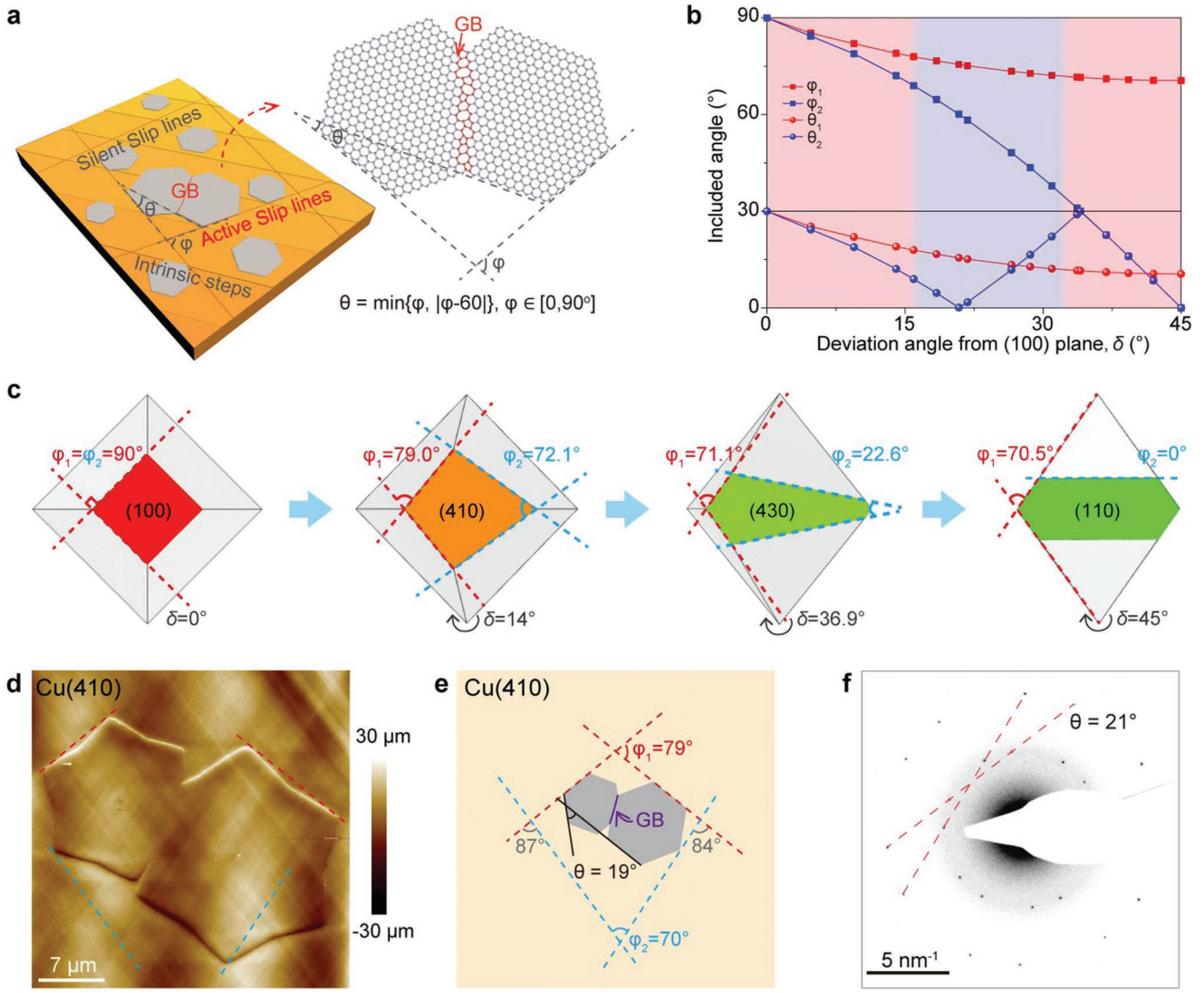

Figure 4. Engineering grain-boundary misorientation in bicrystal graphene. a) Schematic illustration of controlling the LM (θ) of the GBs by the AS angle φ on a specific crystal facet. b) Plot of φ and θ as a function of δ on Cu($hk0$) facets. c) Schematic illustration of the theoretical AS angle φ on the Cu(100), Cu(410), Cu(430), and Cu(110) facets. d) AFM image of bicrystal graphene with specific LM on the Cu(410) facet. e) Schematic of bicrystal graphene formed on the Cu(410) facet in (d). The active slip lines in (c–e) are highlighted by red dotted lines. f) Corresponding SAED pattern of the GB region with respect to the bicrystal graphene on the Cu(410) facet.

The slip-line-guided growth principle can not only direct the epitaxial growth of single-crystal graphene films, but also tailor the lattice misorientation of GBs in bicrystal graphene,[18–20] which is important for both fundamental research and development of novel nanodevices.[12,21] Intuitively, we can utilize single-crystal Cu foils with at least two sets of active slip lines as growth substrates, where graphene domains with differently designed orientations merge to form specific GB structures. In this case, the lattice misorientation (LM,θ) of the GBs is determined by the included angle of active slip lines (AS angle, φ) and, ultimately, the Miller index of the metal surface (**Figure 4**a). Given the sixfold symmetry of the graphene lattice, the correlation between θ and φ can be expressed as

$$\theta = \min\{\varphi, |\varphi - 60^\circ|\}, \varphi \in [0, 90^\circ] \quad (1)$$

In the case of Cu($hk0$) facets, the four sets of slip lines can be divided into two categories [u,v, ± w_1] and [u,v, ± w_2], which correspond to two possible categories of AS angles φ_1 and φ_2, and two categories of LM angles θ_1 and θ_2. Both the AS angles and LM vary with the change in the deviation angle δ between Cu($hk0$) and Cu(100) (Figure 4b; Table S2, Supporting Information). Whether [u,v, ± w_1] or [u,v, ± w_2] becomes the active slip lines can be roughly determined by comparing their proximity to the <211>/<110> directions (Table S3, Supporting Information), as distinguished by regions with diverse colors in Figure 4b. Figure 4c further elaborates the evolution of the AS angles with the variation in the deviation angle δ on the representative crystal facets of Cu(100) ($\delta = 0°$), Cu(410) ($\delta = 14°$), Cu(430) ($\delta = 36.9°$), and Cu(110) ($\delta = 45°$).

Based on the slip-line-guided growth principle, GBs with LM angles of ≈21° and 11° were successfully constructed on Cu(410) and Cu(430) foils, respectively. In detail, the active slip lines on the Cu(410) surface are along the $[1\bar{4}5]$ and $[1\bar{4}\bar{5}]$ directions, forming an AS angle $\varphi = 79°$ and guiding the construction of the GB with $\theta = 19°$ (Figure 4d,e; Figure S10, Supporting Information), which is very close to the value (21°) measured by SAED characterization (Figure 4f). Analogously, the active slip lines on the Cu(430) surface are along the $[3\bar{4}7]$ and $[3\bar{4}\bar{7}]$ directions, resulting in $\varphi = 71°$ and $\theta = 11°$, which is consistent with the SAED value (11°, Figure S11a–c, Supporting Information). This strategy is also applicable to more general Cu(*hkl*) surfaces. For example, the active slip lines on the Cu(431) surface are along the $[4\bar{5}1]$ and $[4\bar{3}\bar{7}]$ directions, resulting in φ = 47° and θ = 13° (SAED value = 10°, Figure S11d–f, Supporting Information).

3. Conclusion

We have demonstrated the essential role of slip lines in guiding the growth of graphene domains on metal surfaces. The graphene domains tend to align with active slip lines, which have a high binding energy with the graphene edge. For practical applications, a geometrical criterion was proposed to predict the possible crystal orientation of graphene domains on arbitrary crystal facets. Under this guidance, the controllable engineering of lattice misorientation angle of 2D GBs was achieved on the designed metal facets. This work deepens the fundamental understanding of crystal orientation control during 2D materials growth. Our findings could inspire further developments in 2D GB engineering and lead to reliable strategies to control the interlayer twist angles of 2D crystals via CVD.

4. Experimental Section

Preparation of Single-Crystal Cu Foils: The single crystal Cu foils with a series of crystal facets were obtained according to our pre-established method.[14]

Graphene Growth: Graphene was grown on single-crystal Cu foils with a low-pressure CVD system. The as-prepared Cu foils were placed into the tube furnace and then heated to 1020 °C under an 800 sccm flow of Ar, then annealed at 1020 °C for 40 min under an 800 sccm flow of H_2. After annealing, graphene was grown on the surface of Cu foils for 2–10 min under an 800 sccm flow of H_2 and a 0.8 sccm flow of CH_4. During the whole CVD process, the pressure was kept at 2000 Pa.

Graphene Transfer onto TEM Grids: Graphene was transferred onto TEM grids via a polymer-assisted method. The graphene/Cu sample was first spin-coated with poly(methyl methacrylate) (PMMA) at 2000 rpm and then baked at 170 °C for 3 min to form PMMA/graphene/Cu composite. Further, the Cu substrate was etched and removed by $Na_2S_2O_8$ solution (1 mol L^{-1}). After being washed with deionized water, the PMMA/graphene composite layer was subsequently picked up by a TEM grid (QUANTIFOIL Holey Carbon supports). At last, PMMA was dissolved by hot acetone.

Characterization: SEM (Thermo Scientific Quattro S), EBSD (AMETEK EDAX DigitalView EBSD Camera in combination with EDAX's TEAM, under 20 kV), AFM (Bruker Dimension Icon with ScanAsyst mode), TEM (FEI Tecnai F30 operated at 300 kV), and SAED (Gatan GIF994) were employed to analyze the crystal orientation, surface morphology (slip lines) of the as-prepared Cu foils, as well as to character the crystal orientation, grain morphology of the as-grown graphene domains.

Statistical Analysis: The statistical data of orientation angle of graphene domain were measured with SEM images, and then presented in the form of a statistical histogram. The horizontal right direction in the SEM image is designated as the reference orientation (0°). The counterclockwise and clockwise rotations with respect to the reference orientation are designated as positive and negative orientations, respectively. The sample sizes of Figure 1d,g and Figure S8a–f, Supporting Information are 223, 488, 278, 331, 267, 281, 177, and 350, respectively.

Calculations of Binding Energies: To acquire reasonable configurations of the slip lines on Cu substrates, the atomistic models were first optimized by molecular dynamics (MD) simulations before DFT calculations. The interactions between Cu atoms were described by EAM potential.[22] The models of the substrates were relaxed in NPT ensembles at 300 K with zero pressure. Periodic boundary conditions were applied in the Cu(410) plane. The time step is assumed to be 1 fs and the configurations shown in Figure 2g–i were acquired after a relaxation of 50 000-time steps. All the MD simulations were performed using the LAMMPS[23] package and visualized through Ovito.[24] Then DFT calculations for the binding energies between the graphene edges and the surface steps of Cu(410) substrates were performed using the Vienna Ab initio Simulation Package code.[25,26] The projector augmented wave pseudopotentials[27,28] and the generalized gradient approximation of the Perdew–Burke–Ernzerhof functional[29,30] are used. The DFT-D3 van der Waals density functional was used for the corrections of the interlayer van der Waals interaction. A plane-wave basis set with a kinetic-energy cut-off of 520 eV was used for all the interaction calculations. Periodic boundary conditions were applied in the two in-plane directions for all the calculations conducted here. Structural relaxations were performed through a conjugate-gradient algorithm until the atomic forces converged to 0.01 eV. The Monkhorst–Pack grids of *k*-points were $4 \times 1 \times 1$ for all three kinds of substrates in Figure 2.[31] The binding energy $E_{binding}$ between a graphene edge and a Cu step is defined as

$$E_{binding} = -\frac{E_{total} - E_{Cu} - E_C}{L} \quad (2)$$

where E_{Cu}, E_C, and E_{total} refer to the energies of the Cu substrate, graphene ribbon, and the total energy after binding, respectively. L is the length of the graphene ribbon.

Supporting Information

Supporting Information is available from the Wiley Online Library or from the author.

Acknowledgements

Y.L.Z.L., H.Y.L., and Z.H.C. contributed equally to this work. This work was financially supported by National Natural Science Foundation of China (NSFC, Nos. T2188101, 52021006), Beijing National Laboratory for Molecular Science (BNLMS-CXTD-202001), National Key R&D Program of China (Nos. 2016YFA0200101, 2016YFA0200103, and 2018YFA0703502), and the Beijing Municipal Science and Technology Commission (Nos. Z191100000819005, Z191100000819007, and Z201100008720005). Y.W. acknowledges support from the NSFC Basic Science Center for "Multiscale Problems in Nonlinear Mechanics" (No. 11988102).

Conflict of Interest

The authors declare no conflict of interest.

Data Availability Statement

The data that support the findings of this study are available from the corresponding author upon reasonable request.

Keywords

epitaxial growth, grain-boundary engineering, graphene, slip line

Received: February 5, 2022
Revised: April 22, 2022
Published online: June 3, 2022

[1] D. W. Pashley, in *Epitaxial Growth*, Academic Press, Inc., New York **1975**.
[2] Q. Yuan, B. I. Yakobson, F. Ding, *J. Phys. Chem. Lett.* **2014**, *5*, 3093.
[3] X. Zhang, Z. Xu, L. Hui, J. Xin, F. Ding, *J. Phys. Chem. Lett.* **2012**, *3*, 2822.
[4] P. W. Sutter, J.-I. Flege, E. A. Sutter, *Nat. Mater.* **2008**, *7*, 406.
[5] K. V. Bets, N. Gupta, B. I. Yakobson, *Nano Lett.* **2019**, *19*, 2027.
[6] L. Wang, X. Xu, L. Zhang, R. Qiao, M. Wu, Z. Wang, S. Zhang, J. Liang, Z. Zhang, Z. Zhang, W. Chen, X. Xie, J. Zong, Y. Shan, Y. Guo, M. Willinger, H. Wu, Q. Li, W. Wang, P. Gao, S. Wu, Y. Zhang, Y. Jiang, D. Yu, E. Wang, X. Bai, Z.-J. Wang, F. Ding, K. Liu, *Nature* **2019**, *570*, 91.
[7] T.-a. Chen, C.-p. Chuu, C.-c. Tseng, C.-k. Wen, H. S. P. Wong, S. Pan, R. Li, T.-a. Chao, W.-c. Chueh, Y. Zhang, Q. Fu, B. I. Yakobson, W.-h. Chang, L.-j. Li, *Nature* **2020**, *579*, 219.
[8] P. Yang, S. Zhang, S. Pan, B. Tang, Y. Liang, X. Zhao, Z. Zhang, J. Shi, Y. Huan, Y. Shi, S. J. Pennycook, Z. Ren, G. Zhang, Q. Chen, X. Zou, Z. Liu, Y. Zhang, *ACS Nano* **2020**, *14*, 5036.
[9] Q. Ruan, L. Wang, K. V. Bets, B. I. Yakobson, *ACS Nano* **2021**, *15*, 18347.
[10] J. Dong, L. Zhang, X. Dai, F. Ding, *Nat. Commun.* **2020**, *11*, 5862.
[11] R. Wu, Y. Ding, K. M. Yu, K. Zhou, Z. Zhu, X. Ou, Q. Zhang, M. Zhuang, W.-D. Li, Z. Xu, M. S. Altman, Z. Luo, *Chem. Mater.* **2019**, *31*, 2555.
[12] W. Yao, B. Wu, Y. Liu, *ACS Nano* **2020**, *14*, 9320.
[13] W. Callister, *Materials Science and Engineering: An Introduction*, 7th ed., John Wiley & Sons, Inc., Hoboken, NJ, USA **2007**.
[14] Y. Li, L. Sun, Z. Chang, H. Liu, Y. Wang, Y. Liang, B. Chen, Q. Ding, Z. Zhao, R. Wang, Y. Wei, H. Peng, L. Lin, Z. Liu, *Adv. Mater.* **2020**, *32*, 2002034.
[15] Y. Li, L. Sun, H. Liu, Y. Wang, Z. Liu, *Inorg. Chem. Front.* **2021**, *8*, 182.
[16] B. Deng, Z. Pang, S. Chen, X. Li, C. Meng, J. Li, M. Liu, J. Wu, Y. Qi, W. Dang, H. Yang, Y. Zhang, J. Zhang, N. Kang, H. Xu, Q. Fu, X. Qiu, P. Gao, Y. Wei, Z. Liu, H. Peng, *ACS Nano* **2017**, *11*, 12337.
[17] X. Xu, Z. Zhang, J. Dong, D. Yi, J. Niu, M. Wu, L. Lin, R. Yin, M. Li, J. Zhou, S. Wang, J. Sun, X. Duan, P. Gao, Y. Jiang, X. Wu, H. Peng, R. S. Ruoff, Z. Liu, D. Yu, E. Wang, F. Ding, K. Liu, *Sci. Bull.* **2017**, *62*, 1074.
[18] K. V. Bets, V. I. Artyukhov, B. I. Yakobson, *ACS Nano* **2021**, *15*, 4893.
[19] Y. Wei, J. Wu, H. Yin, X. Shi, R. Yang, M. Dresselhaus, *Nat. Mater.* **2012**, *11*, 759.
[20] J. Wu, Y. Wei, *J. Mech. Phys. Solids* **2013**, *61*, 1421.
[21] O. V. Yazyev, Y. P. Chen, *Nat. Nanotechnol.* **2014**, *9*, 755.
[22] S. M. Foiles, M. I. Baskes, M. S. Daw, *Phys. Rev. B* **1986**, *33*, 7983.
[23] S. Plimpton, *J. Comput. Phys.* **1995**, *117*, 1.
[24] A. Stukowski, *Modell. Simul. Mater. Sci. Eng.* **2010**, *18*, 015012.
[25] G. Kresse, J. Furthmüller, *Comput. Mater. Sci.* **1996**, *6*, 15.
[26] G. Kresse, J. Furthmüller, *Phys. Rev. B* **1996**, *54*, 11169.
[27] P. E. Blöchl, *Phys. Rev. B* **1994**, *50*, 17953.
[28] G. Kresse, D. Joubert, *Phys. Rev. B* **1999**, *59*, 1758.
[29] J. P. Perdew, K. Burke, M. Ernzerhof, *Phys. Rev. Lett.* **1996**, *77*, 3865.
[30] J. P. Perdew, K. Burke, M. Ernzerhof, *Phys. Rev. Lett.* **1997**, *78*, 1396.
[31] H. J. Monkhorst, J. D. Pack, *Phys. Rev. B* **1976**, *13*, 5188.